AIAA 2007-2278

Vibration analysis of pretwisted beams for the design of hybrid axial-torsional transducers

Kuang-Chen Liu,* James Friend† and Leslie Yeo‡

Department of Mechanical Engineering, Monash University, Clayton, VIC, 3800, Australia

A new design for hybrid axial-torsional transducers using pretwisted beams requires the resonance frequencies of the torsional and axial vibration modes to be matched. To aid in designing such transducers, the effects of increasing pretwist and changing the cross-section geometry on the resonance frequencies are investigated analytically. The governing equations and boundary conditions for extension, torsion, and cross-sectional warping are derived using the semi-inverse method and Hamilton's principle. A general set of differential equations for the cross-sectional warping of pretwisted beams is derived. Through scaling, the warping function is shown to be locally similar to the Saint-Venant warping function when the beam is slender, low in pretwist, and torsional deformation is dominant. Using this approach, geometric and material limitations in the use of the Saint-Venant's warping function are illustrated, beyond which the simpler form may no longer be used. The simplified equations of motion are solved under the free-free boundary condition for resonance frequencies and mode shapes, and a comparison with finite element analysis illustrates the limitations.

I. Introduction

A key element in the development of various ultrasonic devices is a hybrid axial-torsional piezoelectric transducer, which converts electrical excitations to and from combined axial-torsional vibrations. Applications for these transducers can be found in micro-actuation,[1] ultrasonic welding,[2] and rotary ultrasonic motors.[3]

Conventional hybrid axial-torsional transducers are composed of both axially-poled and circumferentially-poled piezoelectric-ceramic disks. While the design theory is well developed,[3] such transducers are difficult to manufacture due to the need for circumferentially-poled piezoelectric elements.[4] The construction involves cutting a piezoelectric-ceramic ring into small sectors, which are then individually polarized along the circumferential direction, and finally glued back together. A different design by Tsujino[2,5,6] eliminates this problem by using only axially-poled piezoceramic disks, converting the axial vibration into coupled axial-torsional vibration via helically slotted cylinders. The vibration converter approach has been successfully implemented in welding applications, but the helical slots requires CNC machining and presents a major challenge to its miniaturization for wire-bonding and micro-actuation applications.

Friend and his colleagues[1] investigated the use of pretwisted beams as simple vibration converters. Using simple beam theory, the finite-element method, and experiments, they demonstrated the possibility of making practical vibration converters using pretwisted beams. The investigation on the use of pretwisted beams as vibration converters is extended in this paper; the effect of pretwist and cross-sectional geometry on the resonance frequencies and the vibration mode shapes are examined. This is done by deriving the equations of motion and boundary conditions using Hamilton's principle, which is then solved using free-free boundary conditions.

The structural and dynamic behaviour of pretwisted beams has been the subject of extensive research due to its importance as a model for rotor blades.[7] Because of its complex geometry, a number of approximate beam theories have been developed. The static axial-torsional coupling was investigated by Rosen,[8,9] Hodges,[10] Krenk,[11] while the dynamic response was studied by Rosen,[7] Tsuiji,[12] and Curti and Risitano.[13]

*Graduate student, Desk 63 Rm 134 Bldg 37, AIAA Student member, daniel.liu@eng.monash.edu.au

†Associate Professor, Rm 133 Bldg 31.

‡Senior Lecturer, Rm 132 Bldg 31.

In the above works on beam theories (except Ref.13), semi-inverse and variational methods were used to derive the equations of motion. The correctness and complexity of the resulting equations depend crucially on the initial choice of the compatible displacement field. Two major assumptions were made by the previous authors: first, that deformation parallel to the cross-sections is negligible, and second, that axial deformation consists of a bulk displacement u_1 and a cross-sectional warpage given by the Saint-Venant warping function ψ of the same beam with zero pretwist. For example, the displacement field used by Rosen[9] (and Tsuiji[12] if bending is neglected) is

$$u(x,y,z,t) = u_1(x,t) + \phi'(x,t)\psi(x,y,z), \quad (1a)$$
$$v(x,y,z,t) = y[\cos\phi(x,t) - 1] - z\sin\phi(x,t), \quad (1b)$$
$$w(x,y,z,t) = y\sin\phi(x,t) + z[\cos\phi(x,t) - 1], \quad (1c)$$

where u, v, w are, respectively, the displacement components in the x, y, z directions, ϕ represents the angle of elastic rotation (in addition to the pretwist angle β) and the prime denotes differentiation with respect to x (see figure 1).

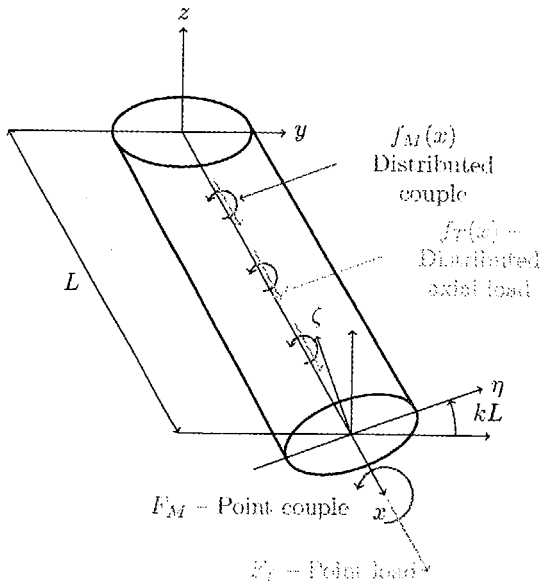

Figure 1. The coordinate systems used to describe the pretwisted beam, and the external forces and moments acting on the beam.

There are two shortcomings in the exisitng work on the vibration of pretwisted beams. The first problem concerns the correct form of the warping function used in Eq.(1). Through an asymptotic solution to the three-dimensional equations of elasticity, Krenk[14] showed that the Saint-Venant warping function was the leading term in the axial-torsional coupling. This provided a justification for the assumed form of Eq.(1) when the pretwist is small, however, it is unclear at what limit the approximation fails.

The second problem concerns the correct form of the strain-displacement relation and the potential energy used to derive the equations of motion. Rosen[9] derived a set of nonlinear static load-deformation relations for the torsion and extension of twisted bars. He assumed that torsion was uniform (i.e. $\frac{\partial^2\phi}{\partial x^2} = 0$), which simplifies the potential energy function considerably. Later, in a review of twisted structures,[7] Rosen derived the equations of motion for the dynamic case by adding inertia terms to the linearized version of the static load-deformation relations. This is equivalent to adding kinetic energy to the potential energy in Ref.9 and applying Hamilton's principle. The equations he obtain has the following form,

$$a_1 u_1'' + a_2\phi'' = \ddot{u},$$
$$b_1 u_1'' + b_2\phi'' = \ddot{\phi}, \quad (2)$$

which is the same as those derived by Tsuiji,[12] and Curti and Risitano[13] except for slight differences in coefficients. The problem with Rosen's approach is that while the assumption of uniform torsion may be valid in the static case, it is not true in the dynamic case.[7] As can be seen in Eq.(2) the ϕ'' terms are clearly not taken to be zero.

In this work, the semi-inverse method and Eq.(1) remain the starting point, however, torsion is not assumed to be uniform, furthermore the complete governing equations for the warping function and equations of motion of a pretwisted beam are sought. The warping function is treated as an unknown, dependent variable in applying Hamilton's principle. Inclusion of the warping function in the variational process results in a new set of governing equations for the warping function. Scaling analysis is then used to quantify the limits under which the Saint-Venant warping function and other simplifying assumptions may be applied. The new equations of motion are then solved to determine how the resonance frequencies are affected by pretwist and the cross-sectional geometry. Note that the present derivation will be limited to linearly elastic and istropic materials and cross-sections with at least two-fold symmetry. This is done so that bending does not appear as a consequence of coupling with torsion and extension.[9]

II. Equations of motion

The equations of motion are derived using Hamilton's principle:

$$\delta \int_{t_1}^{t_2} (T + W_{ext} - U)dt = 0, \tag{3}$$

where T is the kinetic energy, W_{ext} is the virtual work applied by external forces, and U is the strain energy. Note that the deformed state of the pretwisted beam can be described using two coordinate systems (CS): an orthogonal CS (x, y, z), and a rotating CS (x, η, ζ) where η and ζ rotate with the pretwist angle $\beta(x)$ (see figure 1). In this section the orthogonal CS is used since it allows simpler derivation of the equation of motion. Later a switch is made to the rotating CS where simpler boundary conditions can be used when various sectional integrals involving the warping function need to be evaluated.

A. Describing the motion and the deformation

In order to express the strain energy in terms of the displacement field, Green's strain-displacement relation is used,

$$\epsilon_{ij} = \frac{1}{2}\left[\frac{\partial u_j}{\partial x_i} + \frac{\partial u_i}{\partial x_j} + \frac{\partial u_\alpha}{\partial x_i}\frac{\partial u_\alpha}{\partial x_j}\right]. \tag{4}$$

The resulting strain components are

$$\epsilon_{xx} = \frac{\partial u}{\partial x} + \frac{\partial \theta}{\partial x}\psi + \frac{1}{2}\left[\underline{\left(\frac{\partial u}{\partial x}\right)^2} + r^2\theta^2\right], \tag{5a}$$

$$\epsilon_{xy} = \frac{1}{2}\theta\left[\frac{\partial \psi}{\partial y}\left[1 + \underline{\frac{\partial u}{\partial x}}\right] - z\right], \tag{5b}$$

$$\epsilon_{xz} = \frac{1}{2}\theta\left[\frac{\partial \psi}{\partial z}\left[1 + \underline{\frac{\partial u}{\partial x}}\right] + y\right], \tag{5c}$$

$$\epsilon_{yy} = \frac{1}{2}\theta^2\left[\frac{\partial \psi}{\partial y}\right]^2, \qquad \epsilon_{yz} = \frac{1}{2}\theta^2\left[\frac{\partial \psi}{\partial y}\frac{\partial \psi}{\partial z}\right], \qquad \epsilon_{zz} = \frac{1}{2}\theta^2\left[\frac{\partial \psi}{\partial z}\right]^2, \tag{5d}$$

where

$$\frac{\partial u}{\partial x} = \epsilon_1 + \theta\frac{\partial \psi}{\partial x} + \frac{\partial \theta}{\partial x}\psi, \qquad \epsilon_1 = \frac{\partial u_1}{\partial x}, \qquad \theta = \frac{\partial \phi}{\partial x}, \qquad \text{and} \qquad r^2 = z^2 + y^2. \tag{6}$$

To express the kinetic energy in terms of the displacement field, the velocity vector $\dot{\mathbf{R}}$ of each point in the beam is given by

$$\begin{aligned}\dot{\mathbf{R}} =& \dot{\mathbf{u}} = (\dot{u})\hat{e}_x + (\dot{v})\hat{e}_y + (\dot{w})\hat{e}_z \\ =& (\dot{u}_1 + \dot{\theta}\psi)\hat{e}_x + \dot{\phi}(-y\sin\phi - z\cos\phi)\hat{e}_y + \dot{\phi}(y\cos\phi - z\sin\phi)\hat{e}_z \\ =& (\dot{u}_1 + \dot{\theta}\psi)\hat{e}_x + r\dot{\phi}\left[-(\sin\phi)\hat{e}_r + (\cos\phi)\hat{e}_\phi\right],\end{aligned} \tag{7}$$

where the cartesian unit vectors $(\hat{e}_x, \hat{e}_y, \hat{e}_z)$ are transformed to cylindrical unit vectors $(\hat{e}_x, \hat{e}_r, \hat{e}_\phi)$ for compactness. The relationship between cartesian and cylindrical unit vectors are

$$\hat{e}_r = \frac{1}{r}(y\hat{e}_y + z\hat{e}_z), \qquad \text{and} \qquad \hat{e}_\phi = \frac{1}{r}(-z\hat{e}_y + y\hat{e}_z). \tag{8}$$

B. Scaling and nondimensionalization

There is a need to simplify Eq.(5); when fully expanded, Eq.(5a) has 11 terms, which in turn contributes 66 terms to the strain energy. Hence, scaling is used to determine the terms and the conditions under which some of the terms may be neglected. By dividing each of the three dependent variables (u_1, ϕ, ψ) and the

four independent variables (x, y, z, t) by an appropriate characteristic length scale (denoted with subscript c), the following nondimensionalized variables (denoted with a subscript s) are obtained:

$$u_{1s} = \frac{u_1}{u_{1c}}, \qquad \phi_s = \frac{\phi}{\phi_c}, \qquad \psi_s = \frac{\psi}{\psi_c} = \frac{\psi}{r_c^2}, \tag{9a}$$

$$x_s = \frac{x}{x_c} = \frac{x}{L}, \qquad y_s = \frac{y}{r_c}, z_s = \frac{z}{r_c}, \qquad t_s = \frac{t}{t_c} = \frac{t}{L}\sqrt{\frac{E}{\rho}}, \tag{9b}$$

where $x_c = L$ is the beam length and $y_c = z_c = r_c$ is the radius of the circle inscribing the beam cross-section (chosen to reflect the geometry to the beam); $t_c = L\sqrt{\rho/E}$ is the time scale of the axial resonance frequency of the prismatic beam (chosen as a reference); and $\psi_c = r_c^2$ is estimated from the Saint-Venant warping function of a prismatic elliptical beam[15] (similar estimates are obtained from other cross-sections),

$$\psi_{\text{Ellipse}} = -\frac{a^2 - b^2}{a^2 + b^2} yz = -\frac{1 - (b/a)^2}{1 + (b/a)^2} yz = -Byz, \tag{10}$$

where a and b are the semi-major and semi-minor axes, and $B \in (-1, 1)$ is a dimensionless coefficient. Substituting Eq.(9) into $\psi_c = \psi/\psi_s$ provides the following estimate for the scale of ψ

$$\psi_c = \frac{\psi}{\psi_s} = \frac{-B(r_c y_s)(r_c z_s)}{-B y_s z_s} = r_c^2. \tag{11}$$

The definitions for the characteristic deformations (u_{1c}, ϕ_c) are chosen at a later stage of the derivation to simplify the equations of motion. They are shown here for completeness;

$$u_{1c} = \frac{f_{T0} L^2}{EA}, \quad \text{and} \quad \phi_c = \frac{f_{T0} L^2}{ES_1}, \tag{12}$$

where (f_{T0}, f_{M0}) are the characteristic amplitudes of the distributed axial and torsional loads (f_T, f_M). Note the use of f_{T0} for ϕ_c is intentional.

Applying the change of variables in Eq.(9) to Eq.(5), the terms contributing to strain may be separated into four classes by their nondimensional coefficients (NDCs) as shown in Table 1. Note that the NDCs are obtained by dividing the dimensional coefficient by $\phi_c r_c / L$.

Class	Terms	Coefficients	NDC
I	$\frac{\partial u_1}{\partial x}$	$\frac{u_{1c}}{L}$	$\frac{u_{1c}}{\phi_c r_c}$
II	$\theta\frac{\partial \psi}{\partial x}, \frac{\partial \theta}{\partial x}\psi$	$\frac{\phi_c r_c^2}{L^2}$	$\frac{r_c}{L}$
III	$\frac{1}{2}\theta\psi_y, \frac{1}{2}\theta\psi_z, \frac{1}{2}\theta z, \frac{1}{2}\theta y$	$\frac{1}{2}\frac{\phi_c r_c}{L}$	$\frac{1}{2}$
IV	$\frac{1}{2}r^2\theta^2, \frac{1}{2}\theta^2\psi_y^2, \frac{1}{2}\theta^2\psi_y\psi_z, \frac{1}{2}\theta^2\psi_z^2,$	$\frac{1}{2}\frac{\phi_c^2 r_c^2}{L^2}$	$\frac{1}{2}\frac{\phi_c r_c}{L}$

Table 1. Classification of strain components by their Nondimensional Coefficients (NDCs)

A comparison of the relative magnitude of the NDCs show that if the characteristic axial strain $\epsilon_c = u_c/L$ and the characteristic shear strain $\gamma_c = \phi_c r_c/L$ are small then the underlined terms in Eq.(5) and the Class IV terms can be ignored, thus simplifying the strain components to

$$\epsilon_{xx} = \epsilon_1 + \theta\frac{\partial \psi}{\partial x} + \frac{\partial \theta}{\partial x}\psi, \tag{14a}$$

$$\epsilon_{xy} = \frac{1}{2}\theta\left[\frac{\partial \psi}{\partial y} - z\right], \tag{14b}$$

$$\epsilon_{xz} = \frac{1}{2}\theta\left[\frac{\partial \psi}{\partial z} + y\right], \tag{14c}$$

$$\epsilon_{yy} = \epsilon_{yz} = \epsilon_{zz} = 0. \tag{14d}$$

For example, an aluminium beam ($E = 71$ MPa, $G \simeq 27$ GPa, $\tau_{yield} \simeq 250$ MPa) with an elliptical cross-section satisfies the first condition in the elastic region ($\epsilon_{max} = 9.3 \times 10^{-3}$). Using Saint-Venant's theory of torsion for prismatic beams,[15]

$$\begin{aligned} \tau_{max} &= 2G\frac{a^2 b}{a^2+b^2}\frac{\phi_c}{L} \\ \Rightarrow \quad \frac{\phi_c r_c}{L} &= \frac{\tau_{max}}{2G}\left(\frac{1}{b/a} + b/a\right), \end{aligned} \tag{15}$$

where it is noted that $r_c = a$ (the radius of the inscribing circle), it can be estimated that $\phi_c r_c/L < 0.05$ when the ellipse aspect ratio $b/a > 0.1$. This implies that Eq.(14) may not be valid for extremely thin cross-sections. Note that the same strain components are obtained if an infinitesimal strain-displacement relation is used and the elastic rotation ϕ is limited to small angles (eg. $\phi < 8°$ for 1% error from the trigonometric functions in Eq.(1)).

C. Strain energy, kinetic energy and virtual work

The strain energy function is determined from the simplified strain components in Eq.(14) and the constitutive law for elastic isotropic materials. Since $\epsilon_{yy} = \epsilon_{zz} = \epsilon_{yz} = 0$, the contitutive law is given by:

$$\tau_{xx} = E\epsilon_{xx}, \tag{16a}$$

$$\tau_{xy} = 2G\epsilon_{xy} = G\gamma_{xy}, \tag{16b}$$

$$\tau_{xz} = 2G\epsilon_{xz} = G\gamma_{xz}. \tag{16c}$$

The strain energy is thus

$$\begin{aligned} U &= \iiint_V \frac{1}{2}\tau_{xx}\epsilon_{xx} + \frac{1}{2}\tau_{xy}\gamma_{xy} + \frac{1}{2}\tau_{xz}\gamma_{xz}dV \\ &= \iiint_V \frac{1}{2}E\epsilon_{xx}^2 + 2G(\epsilon_{xy}^2 + \epsilon_{xz}^2)dV, \end{aligned} \tag{17}$$

Substituting Eq.(5) into Eq.(17), the strain energy (in terms of the displacement field) is found to be

$$\begin{aligned} U = \iiint_V &\frac{1}{2}E\left(\epsilon_1^2 + (\theta'\psi)^2 + (\theta\psi')^2\right. \\ &\left. + 2\epsilon_1\theta'\psi + 2\epsilon_1\theta\psi' + 2\theta'\theta\psi'\psi\right) \\ &+ \frac{1}{2}G\theta^2\left[\left(\frac{\partial\psi}{\partial y} - z\right)^2 + \left(\frac{\partial\psi}{\partial z} + y\right)^2\right] dV \end{aligned} \tag{18}$$

The kinetic energy is given by the following integral

$$T = \iiint_V \frac{1}{2}\rho\left|\dot{\mathbf{R}}\right|^2 dV, \tag{19}$$

which, upon the substitution of $\dot{\mathbf{R}}$ from Eq.(7) results in

$$\begin{aligned} T &= \iiint_V \frac{1}{2}\rho\left[(\dot{u}_1 + \dot{\theta}\psi)^2 + r^2\dot{\phi}^2\left(\sin^2\phi + \cos^2\phi\right)\right] dV \\ &= \iiint_V \frac{1}{2}\rho\left[\dot{u}_1^2 + 2\dot{u}_1\dot{\theta}\psi + \dot{\theta}^2\psi^2 + r^2\dot{\phi}^2\right] dV. \end{aligned} \tag{20}$$

The virtual work done by external forces is

$$\begin{aligned} W_{ext} &= \int_{x=0}^{L} F_T\epsilon_1 + F_M\theta + f_T u_1 + f_M\phi \quad dx \\ &= \iiint_V \frac{dF_T}{dA}\epsilon_1 + \frac{dF_M}{dA}\theta + \frac{df_T}{dA}u_1 + \frac{df_M}{dA}\phi dV, \end{aligned} \tag{21}$$

where force $F_T(t)$ and moment $F_M(t)$ are applied at the ends of the beam, and tensile force $f_T(x,t)$ and moment $f_M(x,t)$ are distributed along the axis of the beam.

With the virtual work, kinetic and elastic energies now expressed in terms of three unknown functions u_1, ϕ, and ψ, Hamilton's principle may be applied to derive the equations of motion (for details of the variational calculus see Appendix A). Since there are three dependent variables, there are three governing equations:

$$E\frac{\partial}{\partial x}\left(\epsilon_1 + \theta'\psi + \theta\psi'\right) + \frac{df_T}{dA}(x,t) = \rho\frac{\partial}{\partial t}\left(\dot{u_1} + \dot{\theta}\psi\right), \tag{22a}$$

$$E\frac{\partial}{\partial x}\left(\theta\psi'^2 + \epsilon_1\psi' + \theta'\psi\psi'\right) + G\frac{\partial}{\partial x}\left[\theta\left((\psi_y - z)^2 + (\psi_z + y)^2\right)\right] - E\frac{\partial^2}{\partial x^2}\left(\theta'\psi^2 + \epsilon_1\psi + \theta\psi\psi'\right) + \frac{df_M}{dA}(x,t) = \rho\frac{\partial}{\partial t}\left(r^2\dot{\phi}\right) - \rho\frac{\partial^2}{\partial x\partial t}\left(\dot{u_1}\psi + \dot{\theta}\psi^2\right), \tag{22b}$$

$$\rho\left(\dot{\theta}\dot{u_1} + \dot{\theta}^2\psi\right) - E\left(\theta'^2\psi + \epsilon_1\theta' + \theta\theta'\psi'\right) + E\frac{\partial}{\partial x}\left(\theta^2\psi' + \epsilon_1\theta + \theta\theta'\psi\right) + G\theta^2\underline{\left[\frac{\partial}{\partial y}(\psi_y - z) + \frac{\partial}{\partial z}(\psi_z + y)\right]} = 0, \tag{22c}$$

where the natural boundary conditions over the entire surface of the beam are

$$\oiint\left(-E\left(\epsilon_1 + \theta'\psi + \theta\psi'\right) + \frac{dF_T}{dA}\right)a_{nx}dA = 0, \tag{23a}$$

$$\oiint\left(E\left(\psi\psi''\theta + 2\psi\psi'\theta' + \psi^2\theta'' + \psi u_1''\right) - G\left[(\psi_y - z)^2 + (\psi_z + y)^2\right]\theta - \rho\left(\psi\ddot{u_1} + \psi^2\ddot{\theta}\right) + \frac{dF_T}{dA}\right)a_{nx}dA = 0, \tag{23b}$$

$$\oiint -E\left(\psi^2\theta' + \psi u_1' + \psi\psi'\theta\right)a_{nx}dA = 0, \tag{23c}$$

$$\oiint E\left(\theta^2\psi' + \epsilon_1\theta + \theta\theta'\psi\right)a_{nx} + G\theta^2\underline{\left[(\psi_y - z)\,a_{ny} + (\psi_z + y)\,a_{nz}\right]}dA = 0, \tag{23d}$$

and a_{nx}, a_{ny}, a_{nz} are components of the normal vectors on the surface of the beam.

D. Simplification of the warping function

The underlined terms in Eq.(22c) and Eq.(23d) are the governing equations for the Saint-Venant warping function of a prismatic bar. To determine the conditions under which the extra terms can be neglected for pretwisted beams, Eq.(22c) and Eq.(23d) are scaled by substituting the change of variables defined in Eq.(9). The terms in the resulting equations can be separated into six classes by their NDCs (see Table 2): Class V to VII are terms from Eq.(22c) (nondimensionalized with respect to Coef VII) and Class VIII to X are terms from Eq.(23d) (nondimensionalized with respect to |Coef X|) where

$$|\text{Coef X}| = G\frac{\phi_c^2 r_c}{L^2}a_{nr} \qquad \text{and} \qquad a_{nr} = \sqrt{a_{ny}^2 + a_{nz}^2}. \tag{24}$$

If NDC V, VI, VIII and IX are small relative to unity (in other words, small relaive to NDC VII and X), then Eq.(22c) and Eq.(23d) are simplified to the governing equations of the Saint-Venant warping function

$$\nabla^2\psi = 0,$$
$$\left(\frac{\partial\psi}{\partial y} - z\right)a_{ny} + \left(\frac{\partial\psi}{\partial z} + y\right)a_{nz} = 0 \quad \text{on the cross-section boundary.} \tag{26}$$

NDC V, VI, VIII and IX can be expressed in terms of four nondimensional parameters: the slenderness ratio SL, the amplitude ratio R, the tilt ratio of surface normal vectors TR, and Poisson's ratio ν

$$\text{SL} = \frac{r_c}{L}, \quad \text{R} = \frac{\phi_c r_c}{u_{1c}}, \quad \text{TR} = \frac{a_{nx}}{a_{nr}}, \quad \frac{G}{E} = \frac{1}{2(1+\nu)}. \tag{27}$$

Class	Terms	Coefficients	NDC	
V	$\rho\dot{\theta}\dot{u}_1,$	$\rho\frac{\phi_c u_{1c}}{Lt_c^2},$		
	$E\epsilon_1\theta', E\frac{\partial}{\partial x}(\epsilon_1\theta)$	$E\frac{\phi_c u_{1c}}{L^3}$	$\frac{E}{G}\frac{u_{1c}}{\phi_c r_c}\frac{r_c}{L}$	$\frac{E}{G}\frac{\mathrm{SL}}{\mathrm{R}}$
VI	$\rho\dot{\theta}^2\psi,$	$\rho\frac{\phi_c^2 r_c^2}{L^2 t_c^2},$		
	$E\theta'^2\psi, E\theta\theta'\psi',$			
	$E\frac{\partial}{\partial x}\left(\theta^2\psi'\right), E\frac{\partial}{\partial x}\left(\theta\theta'\psi\right),$	$E\frac{\phi_c^2 r_c^2}{L^4}$	$\frac{E}{G}\frac{r_c^2}{L^2}$	$\frac{E}{G}\mathrm{SL}^2$
VII	$G\theta^2\frac{\partial^2\psi}{\partial y^2}, G\theta^2\frac{\partial^2\psi}{\partial z^2}$	$G\frac{\phi_c^2}{L^2}$	1	1
VIII	$E\epsilon_1\theta a_{nx}$	$E\frac{\phi_c u_{1c}}{L^2}a_{nx}$	$\frac{E}{G}\frac{u_{1c}}{\phi_c r_c}\frac{a_{nx}}{a_{nr}}$	$\frac{E}{G}\frac{\mathrm{TR}}{\mathrm{R}}$
IX	$E\theta^2\psi' a_{nx}, E\theta\theta'\psi a_{nx}$	$E\frac{\phi_c^2 r_c^2}{L^3}a_{nx}$	$\frac{E}{G}\frac{r_c}{L}\frac{a_{nx}}{a_{nr}}$	$\frac{E}{G}\times\mathrm{SL}\times\mathrm{TR}$
X	$G\theta^2(\psi_y - z)a_{ny},$	$G\frac{\phi_c^2 r_c}{L^2}a_{ny},$	$\frac{a_{ny}}{a_{nr}}$	
	$G\theta^2(\psi_z + y)a_{nz},$	$G\frac{\phi_c^2 r_c}{L^2}a_{nz},$	$\frac{a_{nz}}{a_{nr}}$	

Table 2. Classification of the components of Eq.(22c) and Eq.(23d) by their NDC

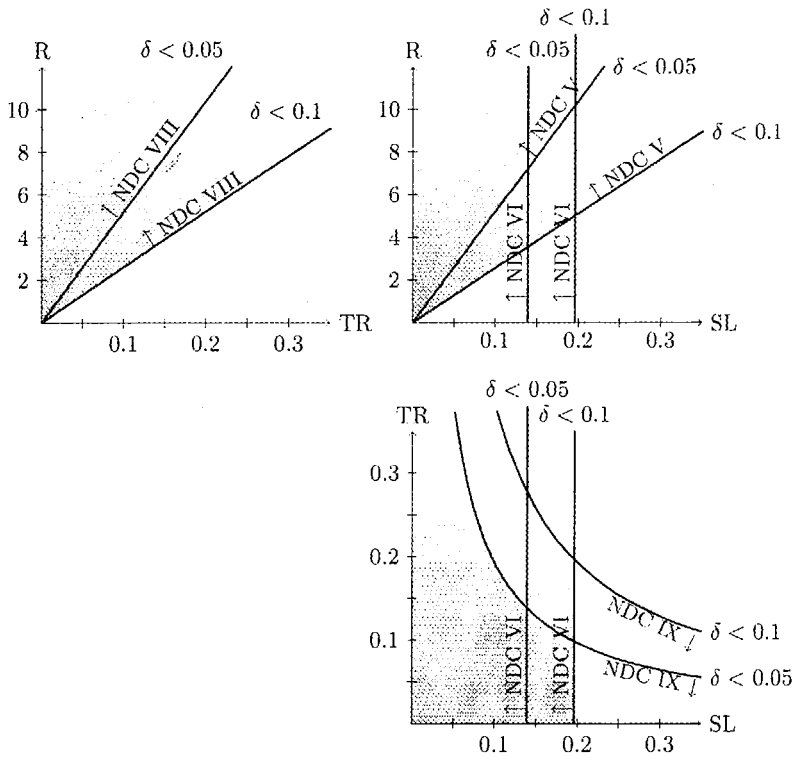

Figure 2. The region in the parameter space (SL, TR, R) where NDC V, VI, VIII and IX are less than δ, representing the criteria under which the simplified warping function Eq.(26) is valid. The region where $\delta = 0.1$ is shaded in gray, and the region where $\delta = 0.05$ is shaded in green.

Choosing NDC $< \delta$ as the criteria under which the simplified warping function is valid, the region in the parameters space (SL, TR, R) where NDC $< \delta$ is true can be plotted for visualization. Note that a Poisson's ratio of 0.3 is chosen since it approximates the behaviour of a wide range of metals. In figure 2 the regions where NDC $< \delta$ for NCD V,VI,VIII,IX are shown by a bounding curve and an arrow, the region where $\delta = 0.1$ is shaded in gray and where $\delta = 0.05$ is shaded in green. The figure shows that there is a flat cap on the slenderness ratio, which means that the approximation is invalid for thick beams. For a beam with rectangular cross-section of width a and height b, the maximum tilt ratio TR is related to slenderness ratio $\mathrm{SL} = r_c/L$, aspect ratio $\mathrm{AR} = b/a$ and pretwist angle $kL = \beta$ by following equation,

$$\mathrm{TR}_{\max} = \frac{k \cdot a}{2} = \frac{k \cdot r_c}{\sqrt{1 + \mathrm{AR}^2}} = \frac{kL \cdot \mathrm{SL}}{\sqrt{1 + \mathrm{AR}^2}}, \tag{28}$$

where $k \cdot r_c = r_c\beta/L$ can be interpreted as a nondimensional rate of pretwist. Note that $\mathrm{TR}_{\max}$ is directly proportional to $k \cdot r_c$, which means that the cap on the allowable tilt ratio sets a maximum pretwist under which the simplified warping function is applicable. The analysis in Appendix B shows the general procedure for determining the tilt ratio of a uniformly twisted beam.

While Eq.(26) appears identical to the governing equations for Saint-Venant's warping function of prismatic bars, there is a subtle difference in the solution. In the present problem, the bar is pretwisted and hence the components of the surface normal vectors (a_{ny}, a_{nz}) are not constant along the beam. By applying a coordinate transformation from the orthorgonal CS (x, y, z) to the rotating CS (x, η, ζ) Eq.(26) is shown to be

$$\begin{aligned} \nabla^2\psi &= 0, \\ \left(\frac{\partial\psi}{\partial\eta} - \zeta\right) a_{n\eta} + \left(\frac{\partial\psi}{\partial\zeta} + \eta\right) a_{n\zeta} &= 0 \\ \text{on the cross-section boundary,} & \end{aligned} \tag{29}$$

where $(a_{n\eta}, a_{n\zeta})$ are now constant. Hence the warping functions from prismatic bars can be applied to pretwisted beams through a simple modification: replacing (y, z) by (η, ζ).

Integrating Eq.(22) and Eq.(23) with respect to the cross-sectional area and applying the change of variables Eq.(12), the equation of motion can be nondimensionalized to the simple form

$$f_{Ts} + \frac{\partial^2 u_s}{\partial x_s^2} + \frac{\partial^2 \phi_s}{\partial x_s^2} = \frac{\partial^2 u_s}{\partial t_s^2}, \tag{30a}$$

$$b_1 f_{Ms} + b_2 \frac{\partial^2 u_s}{\partial x_s^2} + b_3 \frac{\partial^2 \phi_s}{\partial x_s^2} + b_4 \frac{\partial^4 \phi_s}{\partial x_s^4} = b_5 \frac{\partial^2 \phi_s}{\partial t_s^2} - \frac{\partial^4 \phi_s}{\partial t_s^2 \partial x_s^2} + b_6 \frac{\partial^2 u_s}{\partial t_s^2}, \tag{30b}$$

and the natural boundary conditions at $x = 0$ and $x = L$ are

$$\frac{\partial^2 \phi_s}{\partial x_s^2} = 0, \tag{31a}$$

$$\frac{\partial u_s}{\partial x_s} + \frac{\partial \phi_s}{\partial x_s} = \frac{F_T}{f_{T0} L}, \tag{31b}$$

$$\frac{L^2}{K_0}\left(\frac{G}{E} J_s - D_{02}\right) \frac{\partial \phi_s}{\partial x_s} - \frac{\partial^3 \phi_s}{\partial x_s^3} + \frac{\partial^3 \phi_s}{\partial t_s^2 \partial x_s} = \frac{L S_1 F_M}{K_0 f_{T0}}, \tag{31c}$$

where the coefficients are

$$b_1 = \frac{L^2 f_{M0} S_1}{K_0 f_{T0}}, \qquad b_2 = -\frac{S_1^2 L^2}{K_0 A}, \qquad b_3 = \frac{L^2}{K_0}\left(\frac{G}{E} J_s - 2K_1 - 3D_{02}\right), \tag{32a}$$

$$b_4 = -1, \qquad b_5 = \frac{I_p L^2}{K_0}, \qquad b_6 = -\frac{S_1^2 L^2}{K_0 A}. \tag{32b}$$

The sectional integrals $S_1, K_0, K_1, D_{02}, J_s, I_p$ are defined as follows

$$S_i = \iint_A \frac{\partial^i \psi}{\partial x^i} dydz, \tag{33a}$$

$$K_i = \iint_A \left(\frac{\partial^i \psi}{\partial x^i}\right)^2 dydz, \tag{33b}$$

$$D_{ij} = \iint_A \frac{\partial^i \psi}{\partial x^i} \frac{\partial^j \psi}{\partial x^j} dydz, \tag{33c}$$

$$J_s = \iint_A \left(\frac{\partial \psi}{\partial y} - z\right)^2 + \left(\frac{\partial \psi}{\partial z} + y\right)^2 dydz, \tag{33d}$$

$$I_p = \iint_A r^2 dydz \qquad \text{where } i, j = 0, 1, 2, ... \tag{33e}$$

The simple form of Eq.(30) depends on the use of the modified Saint-Venant's warping function, which causes many sectional integrals to vanish due to odd symmetry. For example, $S_i = 0$ when i is even and $D_{ij} = 0$ when i and j are not both even or both odd.

III. Resonance frequency and mode shapes for pretwisted beams with rectangular cross-sections

To test how well the above equations capture the behaviour of pretwisted beams, the resonance frequencies and the corresponding mode shapes for rectangular cross-sectioned beams were solved semi-analytically and compared to the finite-element analysis solution. A simple, free-free boundary condition is used so that Eq.(31) — the natural boundary conditions, and Eq.(30) — the equations of motion are used without the forcing terms f_{Ts}, f_{Ms} or F_T, F_M. To determine the coefficients of Eq.(30), a two term approximation of the warping function for rectangular cross-sections is used[16]

$$\psi(\eta, \zeta) = \eta\zeta - \frac{8a^2}{\pi^3} \frac{\sinh \frac{\pi\zeta}{a}}{\cosh \frac{\pi b}{2a}} \sin \frac{\pi\eta}{a}. \tag{34}$$

Equations (30) and (31) are then fully defined by four nondimensional parameters: ν, the Poisson's ratio; SL, the beam slenderness ratio; AR, the cross-sectional aspect ratio; and kL, the total pretwist angle.

A. Solving the equation of motion

To solve Eqs.(30) and (31) analytically, the solutions are assumed to be of the following form,

$$\begin{aligned} u_s(x.t) &= Ue^{\lambda x_s} e^{i\omega t_s}, \\ \phi_s(x,t) &= \Phi e^{\lambda x_s} e^{i\omega t_s}. \end{aligned} \tag{35}$$

Substituting Eq.(35) into Eq.(30) results in an amplitude ratio R_s,

$$R_s = \frac{\Phi}{U} = -\frac{\lambda^2 + \omega^2}{2\lambda^2}, \tag{36}$$

and a characteristic equation of the form

$$A_1\lambda^6 + (A_2 + A_3\omega^2)\lambda^4 + (A_4 + A_5\omega^4)\lambda^2 + \omega^4 = 0, \tag{37}$$

where the coefficients $A_1, \ldots, A_5$ are combinations of coefficients $b_1, \ldots, b_6$. The characteristic equation has six complex roots

$$\lambda_{1,2} = \pm i\mu_1(\omega), \tag{38a}$$

$$\lambda_{3,4} = \pm i\mu_2(\omega), \tag{38b}$$

$$\lambda_{5,6} = \pm\mu_3(\omega), \tag{38c}$$

where μ_1, μ_2, μ_3 are real-valued functions of ω. The solution thus has the form

$$u_s(x_s,t_s) = [U_1\cos(\mu_1 x_s) + U_2\sin(\mu_1 x_s) + U_3\cos(\mu_2 x_s) + U_4\sin(\mu_2 x_s) + U_5\cosh(\mu_3 x_s) + U_6\sinh(\mu_3 x_s)]\, e^{i\omega t_s}, \tag{39a}$$

$$\phi_s(x_s,t_s) = [R_1U_1\cos(\mu_1 x_s) + R_2U_2\sin(\mu_1 x_s) + R_3U_3\cos(\mu_2 x_s + R_4U_4\sin(\mu_2 x_s) + R_5U_5\cosh(\mu_3 x_s) + R_6U_6\sinh(\mu_3 x_s)]\, e^{i\omega t_s}. \tag{39b}$$

Substituting Eq.(39) into the six boundary conditions in Eq.(31) results in a matrix equation

$$[BC]\mathbf{U} = 0, \tag{40}$$

where $\mathbf{U} = [U_1 ... U_6]^T$ determines the mode shape and $[BC]$ is a 6×6 matrix whose entries are composed of trigonometric and hyperbolic functions of ω. The natural frequencies ω_n are given by the solutions to the transcendental equation

$$\det([BC]) = 0, \tag{41}$$

and the corresponding mode shapes are determined by the null space of Eq.(40) after substituting ω_n back into $[BC]$.

In the present work, the roots of Eq.(41) were found numerically using the secant method. The root-finding algorithm was set to terminate when $\det([BC]) < 10^{-5}$, and the initial root-containing intervals were obtained by plotting $\det(BC)$ and extracting the intervals where a sign change takes place. Due to the presence of hyperbolic functions, numerical evaluation of $\det(BC)$ is highly sensitive to machine round-off errors. The problem was overcome through the use of the arbitrary precision arithmetics of *Mathematica 5.0* (Wolfram Research Inc., Champaign, Illinois). An example of the curve $\det([BC])$ as a function of ω is shown in figure 3.

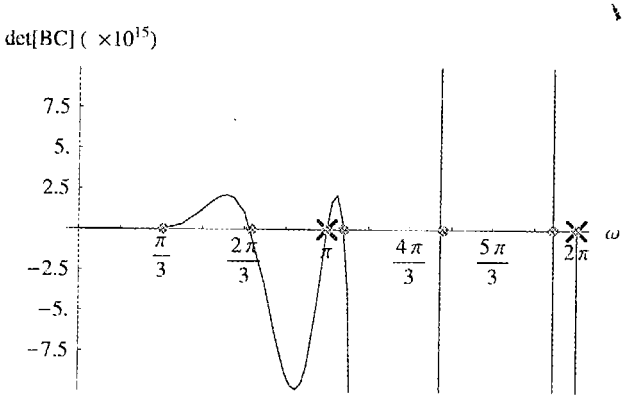

Figure 3. Determining the natural frequencies: the plot of $\det([BC])$ as a function of ω at AR=0.3, SL=0.1, kL=0, $\nu = 0.3$. The roots found from the secant method are marked with red dots. The roots corresponding to integer multiples of π are marked with black crosses.

As a check to the validity of the numerical methods employed, the resonance frequencies predicted by the current method were compared to those predicted by prismatic bar theory. According to the prismatic beam theory the nondimensionalized torsional and axial resonance frequencies $(\omega_{s,T_0}, \omega_{s,A_0})$ are

$$\omega_{s,T_0} = n\pi\sqrt{\frac{GJ_s}{EI_p}}, \qquad n = 1, 2, \ldots \tag{42a}$$

$$\omega_{s,A_0} = m\pi, \qquad m = 1, 2, \ldots. \tag{42b}$$

Integer multiples of π, as marked by the crosses on figure 3, are found to be exact roots of Eq.(41), which agrees with the axial resonance frequencies from Eq.(42b) of prismatic beam theory. The first non-zero root of Eq.(41) is compared with the fundamental torsional frequency predicted by Eq.(42a) in figure 4. It shows agreement between the simple torsion theory and the present theory when pretwist is zero. This result lends credence to the method employed in solving the equations of motion.

A representative set of vibration mode shapes is shown in figure 5, where the mode number n denotes that it corresponds to the n-th non-zero solution to Eq.(41). Whether the n-th root represents an axial or torsional resonance can be inferred from its frequency and the observed mode shape. For example, the vibration mode at $n = 3$ is an axial resonance because it has no torsional motion $\phi = 0$ and $\omega_3 = \pi$ corresponds to the fundamental axial resonance of prismatic bars. The status of the other frequencies is more ambiguous, due to significant coupling between torsional and axial motion, however $n = 1$ can be traced to the fundamental torsional resonance frequency of prismatic bar theory (as shown in figure 4), thus it is predominantly a torsional mode.

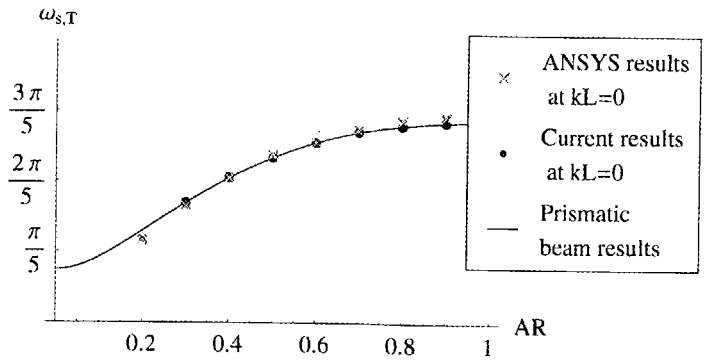

Figure 4. A comparison between the first resonance frequency at kL=0 determined by the analysis presented in this paper and the fundamental torsional resonance frequencies predicted by simple prismatic bar theory.

The variation of the ω_1 torsional resonance as pretwist kL is increased from 0 to 1 revolution was determined for rectangular cross-sections over a wide range of geometries. The beam slenderness ratio ($SL = r_c/L$) was varied from 0.1, 0.05 to 0.025, and the aspect ratio ($AR = b/a =$) was varied from 0.3 to 0.9. The sole relevant material property - Poisson's ratio was fixed at 0.3 as reasoned before. The results for the fundamental torsional resonance $\omega_{s,T}$ are summarized in figure 7.

B. Finite Element Analysis

Finite element modal analysis (FEA) of pretwisted beams were performed using ANSYS 10.0 (ANSYS Inc., Canonsburg, PA USA). The resonance frequencies and the vibration mode shapes were determined over the same range of geometric configurations used for the analytical solutions. In order to automate the identification of the vibration modes of the FEA results — to determine whether the mode is flexural, axial or torsional — a modal identification parameter Λ was defined:[17]

$$\Lambda_i = \frac{1}{S}\oint_s \frac{\mathbf{u}\cdot\mathbf{e}_i}{|\mathbf{u}|}ds, \tag{43}$$

where the path integral is performed along the cross-section perimeter at the beam tip, S is the path length, and i denotes the vibration mode of interest. The parameter Λ_i varies between -1 and 1 and it represents a normalised average of the displacement component in the $\mathbf{e}_i$ direction, where $\mathbf{e}_\phi$ is associated with torsional vibration, and $\mathbf{e}_x$ is associated with axial vibration. In figure 6, the parameters Λ_ϕ and Λ_x are plotted against frequency for the first 30 modes of all geometries considered in the FEA. The path integral for Λ_i was evaluated as a discretized summation over 60 divisions (15 per edge) along the cross-section perimeter. It shows that Λ_ϕ and Λ_x works well as identification parameters for the presence of torsional and axial components in a vibration mode. At low frequencies, the modes are quite distinct and a simple mode classification rule can be used:

- Torsional modes: $|\Lambda_\phi| \geq 0.9$, represented by black dots on figure 6.
- Axial modes: $|\Lambda_x| \geq 0.9$, represented by red boxes on figure 6.
- Flexural modes: $|\Lambda_\phi| \leq 0.1$ and $|\Lambda_x| \leq 0.1$, represented by blue 'x's on figure 6.
- Mixed modes: $0.1 < |\Lambda_\phi| < 0.9$ and $0.1 < |\Lambda_x| < 0.9$, represented by grey '+'s on figure 6.

The first torsional mode for each geometry, as classified by the above scheme, are taken as the fundamental torsional resonance $\omega_{s,T}$. The results are summarized in figure 8.

At higher harmonics, a significant amount of coupling is present for various geometries. Note especially the series of resonance modes that lie along the unit circle on figure 6(c) and form vertical lines at $\omega \simeq 3\pi/2$ on figure 6(a) and (b). These modes belong to geometries with $SL = 0.1$ and $AR \simeq 1$, in other words, thick square beams. Many points in this series are close to the maximum coupling point of $\Lambda_\phi = \Lambda_x = 1/\sqrt{2}$, which makes them promising candidates as vibration converters for the torsional transducer.

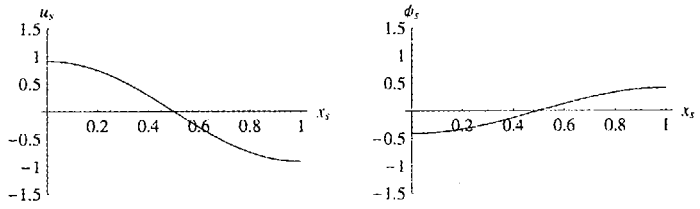

(a) mode number n=1

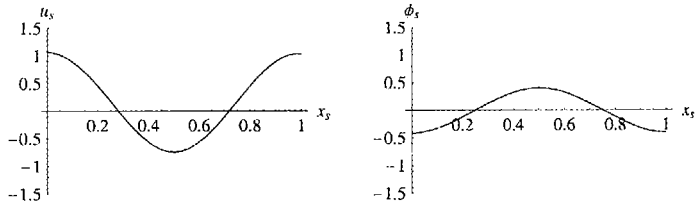

(b) mode number n=2

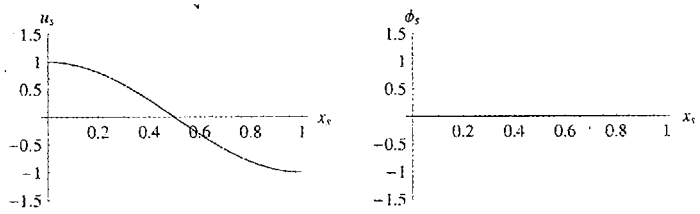

(c) mode number n=3

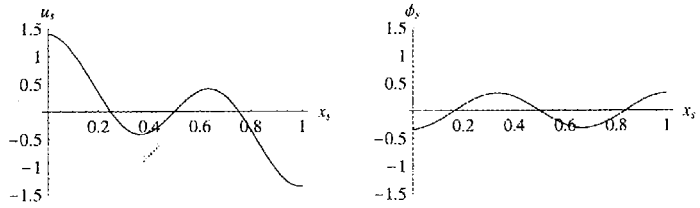

(d) mode number n=4

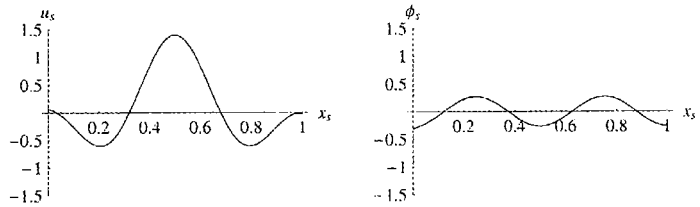

(e) mode number n=5

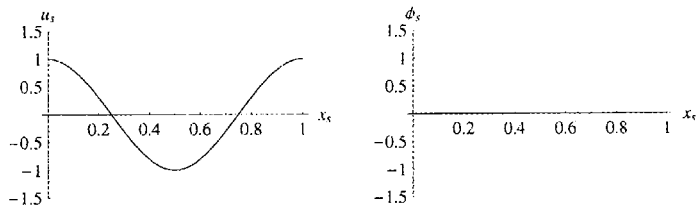

(f) mode number n=6

Figure 5. The vibration mode shapes of an rectangular beam with aspect ratio = 0.4, slenderness ratio = 0.1, pretwist = 0.1 revolution.

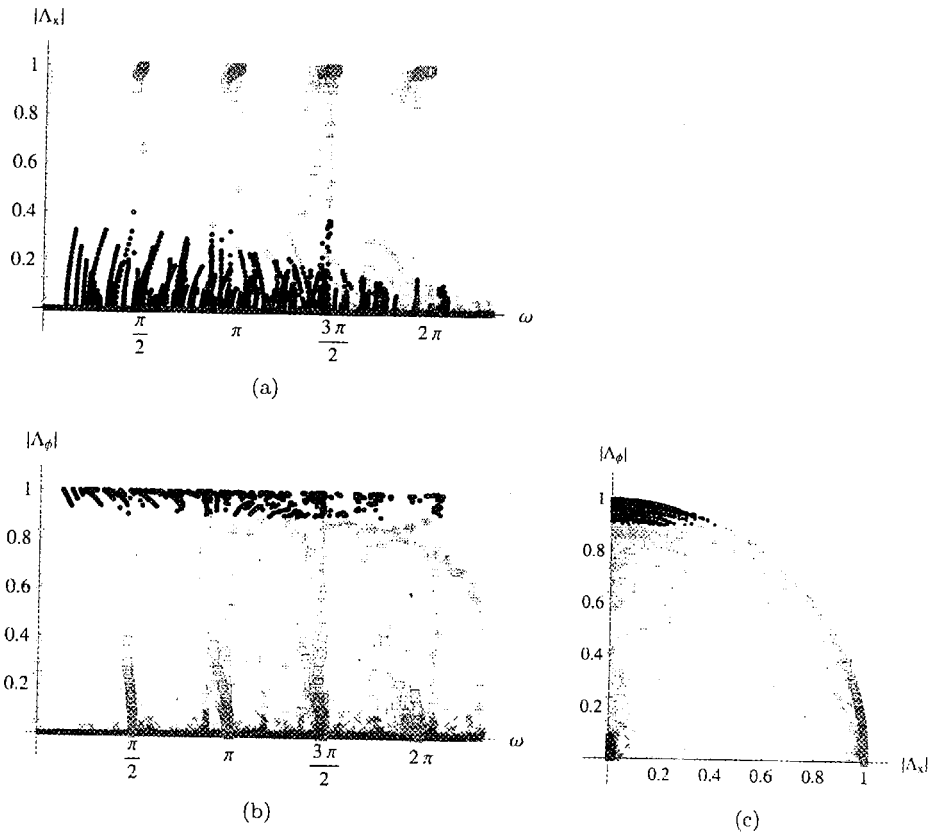

Figure 6. The mode identification parameters Λ_ϕ and Λ_x vs nondimensionalized frequency for the first 30 modes of all geometries considered by FEA. The black dots, red squares, blue x's, and grey plus signs are correspondingly, those points with $|\Lambda_\phi| \geq 0.9$, $|\Lambda_x| \geq 0.9$, $|\Lambda_{\phi,x}| \leq 0.1$ and $0.1 < |\Lambda_{\phi,x}| < 0.9$.

C. Comparison of the theoretical predictions with the FEA results

Figure 7 shows that Eqs. (30) and (31) predict, in general, a fall in $\omega_{s,T}$ as pretwist is increased. Additionally, as the cross-section aspect ratio AR approaches one, $\omega_{s,T}$ rises — as expected from the increased torsional stiffness. However, as the cross-section becomes less elongated, the influence of pretwist on $\omega_{s,T}$ is reduced. On the other hand, the slenderness SL of the beam has little direct influence on $\omega_{s,T}$ when $kL = 0$, but as the beam becomes less slender, the influence of pretwist on $\omega_{s,T}$ is amplified.

Similar trends for the effect of AR and SL on $\omega_{s,T}$ are observed for FEA results on figure 8. As AR is varied from zero to one, $\omega_{s,T}$ increases and becomes less influenced by pretwist. As SL is increased, the effect of pretwist becomes more pronounced. A fundamental difference exists, however, between the theoretical and the FEA results. Instead of a fall in $\omega_{s,T}$, FEA predicts a rise in $\omega_{s,T}$ when pretwist is increased. Note that the trend predicted by FEA agrees with existing experimental results,[7] which show that an increase in pretwist causes a rise in torisonal rigidity and thus a rise in $\omega_{s,T}$.

The discrepancy between the present theory and the FEA result may be traced to simplification of the governing equations for the warping function. The simplification from Eqs.(22c) and (23d) to Eq.(26) holds only if NDC V, VI, VIII and IX are small. Taking NDCs $< \delta$ as the criteria under which Eq.(26) is valid, it may be seen on figure 7 that many points with large pretwist lies outside the valid region. The points marked with black boxes and crosses are, respectively, those points where $0.05 < \delta < 0.104$ and $\delta > 0.104$. The difference between the present theory and the FEA result is significantly reduced within the region where $\delta < 0.05$.

Another source of error is the warping function used for rectangular cross-sections. The solution to

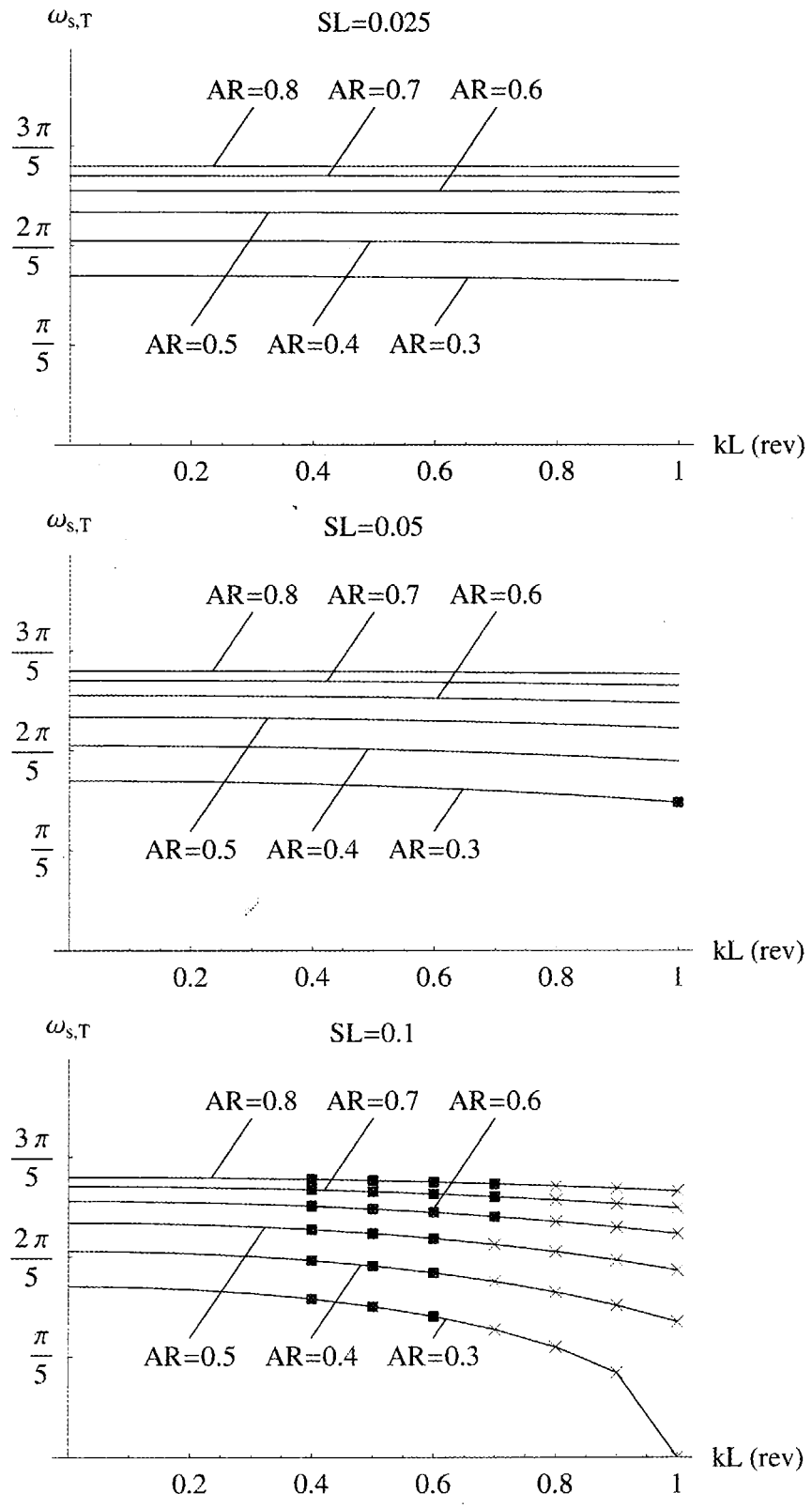

Figure 7. Analytical results for the variation of the fundamental torsional resonance frequency for beams with rectangular cross-sections as pretwist, aspect ratio and slenderness ratio are varied.

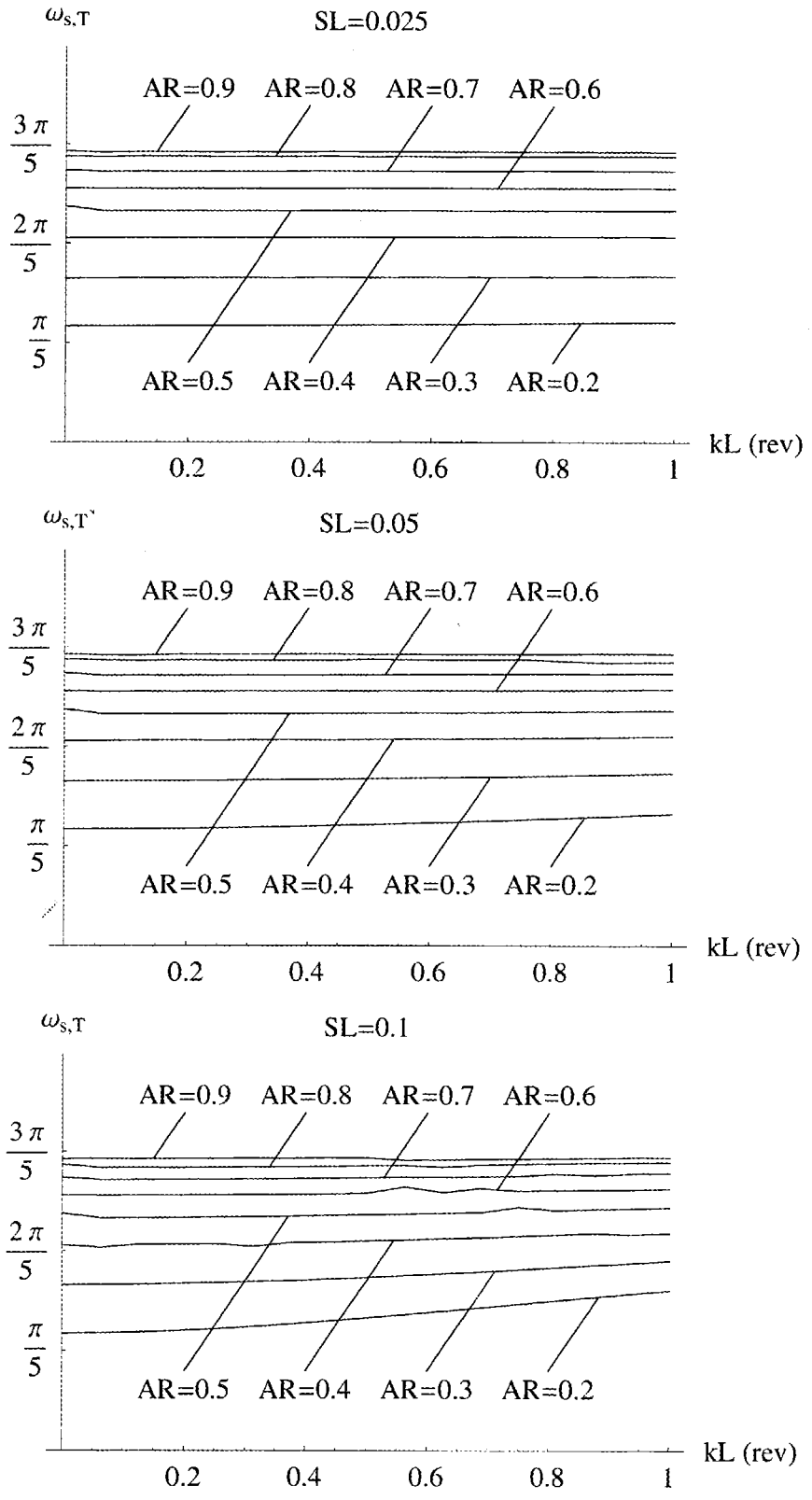

Figure 8. FEM results for the variation of the fundamental torsional resonance frequency for beams with rectangular cross-sections as pretwist, aspect ratio and slenderness ratio are varied.

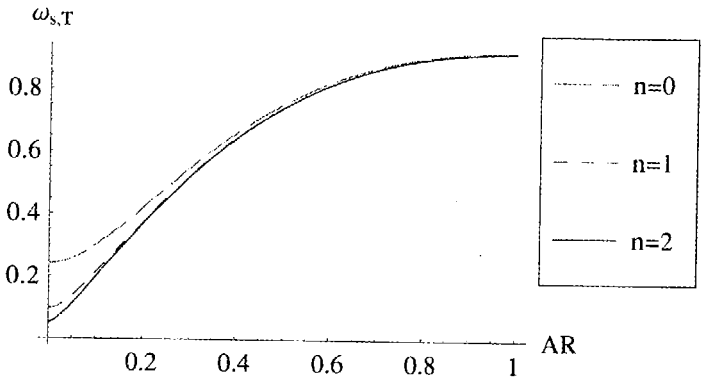

Figure 9. The effect of neglecting higher order terms of the warping function for rectangular cross-sections. The variation of the fundamental torsional resonance frequency $\omega_{s,T}$ predicted by the prismatic bar theory is plotted against AR when the warping function is evaluated to the n-th term.

Eq.(26) for rectangular cross sections with width a and height b is an infinite series[16]

$$\psi(\eta,\zeta) = \eta\zeta - \frac{8a^2}{\pi^3}\sum_{n=0}^{\infty}\frac{(-1)^n}{(2n+1)^3}\frac{\sinh k_n\zeta}{\cosh(k_n b/2)}\sin k_n\eta,$$
$$\text{where} \quad k_n = \frac{(2n+1)\pi}{a}. \tag{44}$$

Due to the complex sectional integrals involved in Eqs.(30)-(33), the warping function was only evaluated to the $n = 0$ term in Section A. The effect of neglecting the higher order terms at zero pretwist can be seen on figure 9, where $\omega_{s,T}$ predicted by prismatic beam theory is plotted against AR as successively more terms are included in ψ. The torsional resonance frequency should approach zero as AR $\to$ 0, however due to the series approximation of ψ, an erroneous finite $\omega_{s,T}$ is predicted. As more terms are included in ψ, the more accurate the $\omega_{s,T}$ predictions become at low AR. While it may appear from figure 9 that the errors caused by the $n = 0$ approximation is negligible when AR > 0.4, it should be noted that only two sectional constants J_s and I_p are involved in the prismatic beam theory. In the present theory, with non-zero pretwist and other sectional constants, predictions at higher AR may also be affected.

IV. Conclusions

A new set of governing equations for the warping function, and the axial and torsional displacement of a pretwisted beam was derived. The conditions under which the modified Saint-Venant warping function is valid for a pretwisted beam was shown to be when the beam is slender, the pretwist is small, and the vibration is torsionally dominant. For rectangular cross-sectioned beams outside the region of validity of the equations of motion, the solutions predict a fall in torsional resonance frequency when pretwist is increased, contrary to some previous theories, our computational results, and existing experimental results.

The importance of understanding the assumptions under which the Saint-Venant's warpage function and related equations are found as commonly performed in the literature[7, 12, 13] is illustrated by this discrepancy. Even for the complex derivation shown here, once the simplification to allow use of Saint-Venant's function is made the domain over which the resulting equations may be used becomes quite small, especially in comparison to FEA. However, the theory corresponds to the computational results over this domain. The derivation illustrates a means to further improve and expand the results described in this paper through solution of the more general warpage function described in Eqs. (22c) and (23d) instead of Eq. (26).

For further work on the use of pretwisted beams as vibration converters for hybrid axial-torsional transducers, experimental validation of the FEA results should be performed. When reliable data on the effect of pretwist on resonance frequencies are obtained, they should be compared with predictions from the present theory and also the simpler theories of Rosen, Tsuiji, and Curti and Risitano. Should the simpler theories be found to model the vibration characteristics of pretwisted beams well, harmonic analysis may be performed

to determine the response of pretwisted beams under forced excitation, paving the way towards the design of simple hybrid axial-torsional transducers.

A. Hamilton's principle and the resulting Euler-Lagrange equation

To apply Hamilton's principle, the strain energy Eq.(18), the kinetic energy Eq.(20), and the work done by external loads Eq.(21) are substituted into Eq.(3), resulting in an equation of the form

$$\delta\left(\int_{t_1}^{t_2}\iiint_V F(x,y,z,t,u_1,\phi,\psi)dV\,dt\right)=0, \tag{45}$$

where

$$\begin{aligned}F(x,y,z,t,u_1,\phi,\psi) = &\\ &\frac{1}{2}E\left(\epsilon_1^2+(\theta'\psi)^2+(\theta\psi')^2+2\epsilon_1\theta'\psi+2\epsilon_1\theta\psi'+2\theta'\theta\psi'\psi\right)\\ &+\frac{1}{2}G\theta^2\left[\left(\frac{\partial\psi}{\partial y}-z\right)^2+\left(\frac{\partial\psi}{\partial z}+y\right)^2\right]\\ &+\frac{1}{2}\rho\left[\dot{u}_1^2+2\dot{u}_1\dot{\theta}\psi+\dot{\theta}^2\psi^2+r^2\dot{\phi}^2\right]\\ &+\frac{dF_T}{dA}\epsilon_1+\frac{dF_M}{dA}\theta+\frac{df_T}{dA}u_1+\frac{df_M}{dA}\phi.\end{aligned} \tag{46}$$

The Euler-Lagrange equation resulting from Eq.(45) is

$$\int_{t_1}^{t_2}\iiint_V \eta_{u_1}\left[\frac{\partial F}{\partial u_1}-\frac{\partial}{\partial x}\left(\frac{\partial F}{\partial \epsilon_1}\right)-\frac{\partial}{\partial t}\left(\frac{\partial F}{\partial \dot{u}_1}\right)\right]dV\,dt$$
$$+\int_{t_1}^{t_2}\oiint \eta_{u_1}\frac{\partial F}{\partial\epsilon_1}a_{nx}dA\,dt+\iiint_V \eta_{u_1}\frac{\partial F}{\partial\dot{u}_1}\bigg|_{t_1}^{t_2}dV=0 \tag{47a}$$

$$\int_{t_1}^{t_2}\iiint_V \eta_\phi\left[\frac{\partial F}{\partial\phi}-\frac{\partial}{\partial x}\left(\frac{\partial F}{\partial\theta}\right)-\frac{\partial}{\partial t}\left(\frac{\partial F}{\partial\dot{\phi}}\right)+\frac{\partial^2}{\partial x^2}\left(\frac{\partial F}{\partial\theta'}\right)+\frac{\partial^2}{\partial x\partial t}\left(\frac{\partial F}{\partial\dot{\theta}}\right)\right]dV\,dt+\iiint_V \eta_\phi\frac{\partial F}{\partial\dot{\phi}}\bigg|_{t_1}^{t_2}dV$$
$$+\int_{t_1}^{t_2}\oiint\left(\eta_\phi\left[\frac{\partial F}{\partial\theta}-\frac{\partial}{\partial x}\left(\frac{\partial F}{\partial\theta'}\right)-\frac{\partial}{\partial t}\left(\frac{\partial F}{\partial\dot{\theta}}\right)\right]a_{nx}+\eta'_\phi\frac{\partial F}{\partial\theta'}a_{nx}\right)dA\,dt+\iiint_V \eta'_\phi\frac{\partial F}{\partial\dot{\theta}}\bigg|_{t_1}^{t_2}dV=0 \tag{47b}$$

$$\int_{t_1}^{t_2}\iiint_V \eta_\psi\left[\frac{\partial F}{\partial\psi}-\frac{\partial}{\partial x}\left(\frac{\partial F}{\partial\psi_x}\right)-\frac{\partial}{\partial y}\left(\frac{\partial F}{\partial\psi_y}\right)+\frac{\partial}{\partial z}\left(\frac{\partial F}{\partial\psi_z}\right)\right]dV\,dt$$
$$+\int_{t_1}^{t_2}\oiint \eta_\psi\left(\frac{\partial F}{\partial\psi_x}a_{nx}+\frac{\partial F}{\partial\psi_y}a_{ny}+\frac{\partial F}{\partial\psi_z}a_{nz}\right)dA\,dt=0, \tag{47c}$$

where $\eta_{u_1},\eta_\phi,\eta_\psi$ represents three independent arbitrary functions and the variational derivatives of F are

$$\frac{\partial F}{\partial u_1}=\frac{df_T}{dA},\qquad \frac{\partial F}{\partial\epsilon_1}=-E(\epsilon_1+\theta'\psi+\theta\psi')+\frac{dF_T}{dA},\qquad \frac{\partial F}{\partial\dot{u}_1}=\rho(\dot{u}_1+\dot{\theta}\psi), \tag{48a}$$

$$\frac{\partial F}{\partial\phi}=\frac{df_M}{dA},\qquad \frac{\partial F}{\partial\theta}=-E(\theta\psi'^2+\epsilon_1\psi'+\theta'\psi\psi')-G\theta\left[(\psi_y-z)^2+(\psi_y+z)^2\right]+\frac{dF_M}{dA},$$
$$\frac{\partial F}{\partial\dot{\phi}}=\rho r^2\dot{\phi},\qquad \frac{\partial F}{\partial\theta'}=-E(\theta'\psi^2+\epsilon_1\psi+\theta\psi\psi'),\qquad \frac{\partial F}{\partial\dot{\theta}}=\rho(\dot{u}_1\psi+\dot{\theta}\psi^2), \tag{48b}$$

$$\frac{\partial F}{\partial\psi}=\rho(\dot{\theta}\dot{u}_1+\dot{\theta}^2\psi)-E(\theta'^2\psi+\epsilon_1\theta'+\theta\theta'\psi'),\qquad \frac{\partial F}{\partial\psi'}=-E(\theta^2\psi'+\epsilon_1\theta+\theta\theta'\psi),$$
$$\frac{\partial F}{\partial\psi_y}=-G\theta^2(\psi_y-z),\qquad \frac{\partial F}{\partial\psi_z}=-G\theta^2(\psi_z+y). \tag{48c}$$

Subsitituting Eq.(48) into the Euler-Lagrange equation Eq.(47) gives the equatons of motion and the boundary conditions.

B. Normal vectors on the surface of pretwisted beams

The surface of a constant cross-section pretwisted beam can be described by the following position vector

$$\mathbf{r}(x,s) = x\mathbf{e}_x + \mathbf{\Gamma}(s), \tag{49}$$

where $\mathbf{\Gamma}(s)$ traces the perimeter of the cross-sectional geometry with the path variable s

$$\begin{aligned}\mathbf{\Gamma}(s) &= \eta(s)\mathbf{e}_\eta + \zeta(s)\mathbf{e}_\zeta \\ &= (\eta(s)\cos kx - \zeta(s)\sin kx)\mathbf{e}_y + (\eta(s)\sin kx + \zeta(s)\cos kx)\mathbf{e}_z.\end{aligned} \tag{50}$$

Normal vectors can be obtained from the cross product of two non-parallel tangent vectors to the surface of the pretwisted beam, thus

$$\mathbf{n} = \frac{\partial \mathbf{r}}{\partial s} \times \frac{\partial \mathbf{r}}{\partial x}. \tag{51}$$

Expressing Eq.(49) in vector form,

$$\mathbf{r}(x,s) = \begin{bmatrix} x\mathbf{e}_x \\ \eta\cos kx - \zeta\sin kx \\ \eta\sin kx + \zeta\cos kx \end{bmatrix}, \tag{52}$$

the tangent vectors are obtained as

$$\frac{\partial \mathbf{r}}{\partial s}(x,s) = \begin{bmatrix} 0 \\ \eta'\cos kx - \zeta'\sin kx \\ \eta'\sin kx + \zeta'\cos kx \end{bmatrix}, \quad \text{and} \quad \frac{\partial \mathbf{r}}{\partial x}(x,s) = \begin{bmatrix} 1 \\ -k(\eta\sin kx + \zeta\cos kx) \\ k(\eta\cos kx - \zeta\sin kx) \end{bmatrix}. \tag{53}$$

Substituting Eq.(53) into Eq.(51) yields

$$\mathbf{n} = \begin{bmatrix} k(\eta\eta' + \zeta\zeta') \\ \eta'\sin kx + \zeta'\cos kx \\ -\eta'\cos kx + \zeta'\sin kx \end{bmatrix}, \tag{54}$$

which can then be used to detrmine the components of the unit normal vector $\hat{\mathbf{n}}$:

$$\hat{\mathbf{n}} = \frac{\mathbf{n}}{|\mathbf{n}|} = [a_{nx}, a_{ny}.a_{nz}]^T. \tag{55}$$

From Eq.(54), the component of the unit normal vector in the radial direction a_{nr} is

$$a_{nr} = \sqrt{a_{ny}^2 + a_{nz}^2} = \frac{1}{|\mathbf{n}|}\sqrt{(\eta')^2 + (\zeta')^2}, \tag{56}$$

which can be used to determine the the following ratios, which is needed for comparing the magnitude of the NDCs in Table 2

$$\frac{a_{nx}}{a_{nr}} = \frac{k(\eta\eta' + \zeta\zeta')}{\sqrt{(\eta')^2 + (\zeta')^2}}, \tag{57a}$$

$$\frac{a_{ny}}{a_{nr}} = \frac{\eta'\sin kx + \zeta'\cos kx}{\sqrt{(\eta')^2 + (\zeta')^2}}, \tag{57b}$$

$$\frac{a_{nz}}{a_{nr}} = \frac{-\eta'\cos kx + \zeta'\sin kx)}{\sqrt{(\eta')^2 + (\zeta')^2}}. \tag{57c}$$

A. Elliptical cross-section

For a beam with an elliptical cross-section

$$\eta(s) = a\cos(s), \qquad \eta'(s) = -a\sin(s), \tag{58}$$

$$\zeta(s) = b\sin(s), \qquad \zeta'(s) = b\cos(s). \tag{59}$$

Substituting Eq.(58) into Eq.(57a) yields

$$\frac{a_{nx}}{a_{nr}} = \frac{k(b^2-a^2)\cos(s)\sin(s)}{\sqrt{a^2\sin^2(s)+b^2\cos^2(s)}}, \tag{60}$$

$$\frac{a_{ny}}{a_{nr}} = \frac{-a\sin^2(s)+b\cos^2(s)}{\sqrt{a^2\sin^2(s)+b^2\cos^2(s)}}, \tag{61}$$

$$\frac{a_{ny}}{a_{nr}} = \frac{-a\sin(s)\cos(s)+b\cos(s)\sin(s)}{\sqrt{a^2\sin^2(s)+b^2\cos^2(s)}}. \tag{62}$$

The extreme values of a_{nx}/a_{nr} are determined by solving for the stationary points of Eq.(60)

$$\frac{d}{ds}\left(\frac{a_{nx}}{a_{nr}}\right) = \frac{(b^2-a^2)k(b^2\cos^4(s)-a^2\sin^4(s))}{\sqrt{b^2\cos^2(s)+a^2\sin^2(s)}} = 0, \tag{63}$$

which has the solution

$$s = \tan^{-1}(\sqrt{b/a}) = \tan^{-1}(\sqrt{\mathrm{AR}}).$$

Substituting Eq.(64) back into Eq.(60) gives the extreme values of a_{nx}/a_{nr} for a beam with elliptical cross section

$$\left(\frac{a_{nx}}{a_{nr}}\right)_{\text{extreme}} = k(b-a) = kL \times \mathrm{SL}(\mathrm{AR}-1). \tag{64}$$

B. Rectangular cross-section

For a beam with a rectangular cross-section of width a and height b, the boundary path can be parameterized as,

$$\eta(s) = \begin{cases} -(a/2)(-1+2s) & , \quad s \in (0,1) \\ -a/2 & , \quad s \in (1,2) \\ (a/2)(-5+2s) & , \quad s \in (2,3) \\ a/2 & , \quad s \in (3,4) \end{cases} \quad \Rightarrow \quad \eta'(s) = \begin{cases} -a & , \quad s \in (0,1) \\ 0 & , \quad s \in (1,2) \\ a & , \quad s \in (2,3) \\ 0 & , \quad s \in (3,4) \end{cases}$$

$$\zeta(s) = \begin{cases} b/2 & , \quad s \in (0,1) \\ (b/2)(3-2s) & , \quad s \in (1,2) \\ -b/2 & , \quad s \in (2,3) \\ -(b/2)(7-2s) & , \quad s \in (3,4) \end{cases} \quad \Rightarrow \quad \zeta'(s) = \begin{cases} 0 & , \quad s \in (0,1) \\ -b & , \quad s \in (1,2) \\ 0 & , \quad s \in (2,3) \\ b & , \quad s \in (3,4) \end{cases} \tag{65}$$

Substituting Eq.(65) into the first of Eq.(57a) yields

$$\frac{a_{nx}}{a_{nr}} = \begin{cases} -k(a/2)(1-2s) & , \quad s \in (0,1) \\ -k(b/2)(3-2s) & , \quad s \in (1,2) \\ -k(a/2)(5-2s) & , \quad s \in (2,3) \\ -k(b/2)(7-2s) & , \quad s \in (3,4) \end{cases} \tag{66}$$

It is clear from Eq.(66) that the extreme values of a_{nx}/a_{nr} occurs at the corners of the cross-sections. Since $b \le a$, the maximum tilt ratio for a rectangular cross-section is

$$\frac{a_{nx}}{a_{nr}} = \frac{k \times a}{2} = \frac{k \times r_c}{\sqrt{1+\mathrm{AR}^2}} = \frac{kL \times \mathrm{SL}}{\sqrt{1+\mathrm{AR}^2}} \tag{67}$$

References

[1]J. R. Friend, K. Nakamura, S. Ueha, Torsional transducers using asymmetrically twisted bars, Proceedings of the 18th International Congress on Acoustics 3 (2004) 2251–2254, kyoto, Japan.

[2]J. Tsujino, T. Ueoka, T. Kashino, F. Sugahara, Transverse and torsional complex vibration systems for ultrasonic seam welding of metal plates, Ultrasonics 38 (1) (2000) 67–71.

[3]K. Nakamura, M. Kurosawa, S. Ueha, Design of a hybrid transducer type ultrasonic motor, IEEE Transactions on Ultrasonics, Ferroelectrics, and Frequency control 40 (4) (1993) 395–400.

[4]S. Lin, Sandwiched piezoelectric ultrasonic transducers of longitudinal-torsional compound vibrational modes, IEEE Transactions on Ultrasonics, Ferroelectrics and Frequency Control 44 (6) (1997) 1189–1197.

[5]J. Tsujino, R. Suzuki, H. Yasojima, Load characteristics of ultrasonics rotary motor using a longitudinal-torsional vibration converter, IEEE Ultrasonic Symposium (1996) 377–382.

[6]J. Tsujino, Ultrasonic motor using a one-dimensional longitudinal-torsional vibration converter with diagonal slit, Smart Materials and Structures 7 (3) (1998) 345–351.

[7]A. Rosen, Structural and dynamic behaviour of pretwisted rods and beams, Applied Mechanics Review 44 (12) (1991) 483–515, part 1.

[8]A. Rosen, The effect of inital twist on the torsional rigidity of beams – another point of view, Journal of Applied Mechanics 47 (1980) 389–392.

[9]A. Rosen, Theoretical and experimental investigation of the nonlinear torsion and extension of initially twisted bars, Journal of Applied Mechanics 50 (1983) 321–326.

[10]A. H. Hodges, Torsion of pretwisted beams due to axial loading, Journal of Applied Mechanics 47 (1980) 393–397.

[11]S. Krenk, A linear theory for pretwisted elastic beams, Journal of Applied Mechanics 50 (1983) 137–142.

[12]T. Tsuiji, Free vibrations of thin-walled pretwisted beams, Bulletin of JSME 28 (239) (1985) 894–898.

[13]G. Curti, A. Risitano, Coupled free, torsional and axial vibration of pre-twisted bars, Meccanica (1979) 157–162.

[14]S. Krenk, The torsion-extension coupling in pretwisted elastic beams, International Journal of Solids and Structures 19 (1) (1983) 67–72.

[15]Y.-C. Fung, Foundations of solid mechanics, Prentice-Hall, 1965.

[16]I. S. Sokolnikoff, Mathematical Theory of Elasticity, McGraw-Hill Book Company, H 531.38 S683M2, 1956.

[17]J. Friend, K. Nakamura, S. Ueha, A torsional transducer through in-plane shearing of paired planar piezoelectric elements, IEEE Transactions on Ultrasonics, Ferroelectrics, and Frequency Control 51 (7) (2004) 871–878.